Broadband near-Infrared Sensitization of Visible Upconversion Luminescence in V^{3+} and Mo^{3+} Co-Doped Cs_2NaYCl_6

Oliver S. Wenger and Hans U. Güdel*

Departement für Chemie und Biochemie, Universität Bern, Freiestrasse 3, CH-3000 Bern 9, Switzerland

Received: April 29, 2002; In Final Form: July 5, 2002

Crystals of Cs_2NaYCl_6 singly doped with Mo^{3+} or V^{3+} and a series of V^{3+}:Mo^{3+} codoped Cs_2NaYCl_6 crystals were studied by low-temperature optical absorption and luminescence spectroscopy with particular focus on their near-infrared (NIR) to visible (vis) photon upconversion properties. In the codoped crystals 15 K Mo^{3+} $^2T_{2g} \rightarrow {}^4A_{2g}$ upconversion luminescence around 14300 cm^{-1} is not only observed after direct excitation into the weak and narrow Mo^{3+} ^2E_g and $^2T_{1g}$ ground-state absorptions around 9700 cm^{-1}, but also after excitation into the broad V^{3+} $^3T_{1g} \rightarrow {}^3T_{2g}$ absorption band between 10000 and 12500 cm^{-1}. This is because the excitation energy is transferred from V^{3+} $^1T_{2g}$ to Mo^{3+} ^2E_g, and this process is studied as a function of the relative V^{3+} and Mo^{3+} dopant concentrations. The Mo^{3+} $^2T_{2g}$ higher excited-state luminescence is not affected by the V^{3+} codopants, and this is because neither of the Mo^{3+} $^2T_{2g}$ emissions spectrally overlaps with V^{3+} absorption. The upconversion mechanisms which are active in the V^{3+}:Mo^{3+} codoped Cs_2NaYCl_6 crystals at 15 K are identified on the basis of one- and two-color upconversion luminescence excitation spectroscopy. V^{3+} is found not only to act as a sensitizer for Mo^{3+} ^2E_g, but also to participate in a nonradiative energy transfer upconversion (ETU) process. At 15 K, there is a strong spectral overlap of V^{3+} $^3T_{1g} \rightarrow {}^3T_{2g}$ ground-state absorption (GSA) with Mo^{3+} $^2E_g \rightarrow {}^4T_{2g}$ excited-state absorption (ESA), leading to efficient GSA/ESA upconversion in 0.8% V^{3+}:0.3% Mo^{3+}:Cs_2NaYCl_6 at 15 K. Excitation with the broadband NIR output of a tungsten lamp induces more than an order of magnitude more 15 K vis upconversion luminescence in 0.8% V^{3+}:0.3% Mo^{3+}:Cs_2NaYCl_6 than in purely 0.3% Mo^{3+} doped Cs_2NaYCl_6.

I. Introduction

In recent years there has been a continuing interest in the development of efficient new nonlinear optical materials. In this field, research has largely focused on second-harmonic generation (SHG), two-photon absorption (TPA), and luminescence upconversion. Among these three fundamentally different processes, SHG has until now found most widespread commercial application.[1] It is used, for example, to convert the near-infrared (NIR) output from both pulsed and continuous-wave Nd^{3+} lasers into green laser radiation.[2] TPA is used as a tool to detect NIR laser pulses in the field of the so-called ultrafast spectroscopy.[3] To date, luminescence upconversion processes were exploited to build several NIR pumped solid-state lasers, which emit in the visible (vis) spectral region.[4−7] Further applications are IR quantum counters, display phosphors, and a three-dimensional imaging display.[8,9] Upconversion is different from SHG and TPA in that it requires at least two metastable excited states: one serving as an energy storage reservoir, typically located in the NIR spectral region, and one which emits the upconverted energy, typically in the vis.[10,11] In efficient upconversion materials the lifetimes of these metastable states are on the order of 10^{-5}−10^{-1} s.[12] Thus, a very stringent selection criterium is imposed on upconversion candidate systems. On the other hand, upconversion processes do not require coherent input radiation. Therefore, upconversion materials have application potential as luminescent materials for enhancing the efficiency of fluorescence lamps by converting their undesired (broadband) NIR output into vis radiation.[13] Most upconversion materials explored to date involve rare earth ions, in particular trivalent lanthanides.[12,14] These ions have multiple metastable excited states when doped into appropriate host lattices,[15] because their spectroscopically active 4f electrons are shielded from their chemical environment by the 5d electrons.[16] Intraconfigurational f−f excitations are thus characterized by small Huang−Rhys parameters, i.e., low electron−phonon coupling and low multiphonon relaxation rate constants.[17] Recently discovered transition metal based upconversion systems exploit the fact that for intraconfigurational d−d transitions, an analogous situation can occur:[18] In octahedral hexa-chloro and -bromo coordination, the d^3 ions Mo^{3+} and Re^{4+} as well as the d^4 ion Os^{4+} all have at least 2 metastable excited states at cryogenic temperatures.[19−23] This is because their lowest energetic excitations all occur within the t_{2g}^3 and t_{2g}^4 electron configurations,[24] respectively, and their electron−phonon coupling is similarly low as for f−f excitations in the lanthanides. In addition, these formally spin-forbidden transitions have oscillator strengths on the order of 10^{-8}−10^{-6}.[25] Thus Mo^{3+}-, Re^{4+}-, and Os^{4+}-based upconversion materials show great similarities to rare earth upconverters in that they have comparable absorption bandwidths, oscillator strengths, and excited-state lifetimes.[26−28] Whereas their long lifetimes are beneficial for upconversion processes, the weak and narrow absorption lines are a disadvantage for the possible incorporation of these materials into lamp phosphors: Only a very limited wavelength range of NIR radiation is absorbed, and this absorption process is rather inefficient.

It is thus of great interest to sensitize upconversion via efficient NIR absorbers. A commonly used ion in this context

* To whom correspondence should be addressed. Fax: ++41 31 631 43 99. E-mail: guedel@iac.unibe.ch.

10.1021/jp021076f CCC: $22.00
Published on Web 09/06/2002

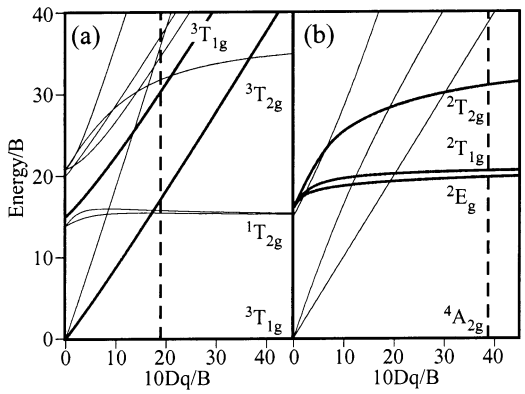

Figure 1. Tanabe−Sugano energy level diagrams for octahedrally coordinated d^2 and d^3 ions. The dashed vertical lines indicate the $10Dq/B$ ratios for (a) V^{3+} and (b) Mo^{3+} in Cs_2NaYCl_6.

is Yb^{3+}, which absorbs radiation around 1 μm very efficiently. It has been successfully used to induce and to enhance upconversion in a variety of systems, e.g., Yb^{3+}/Er^{3+},[29] Yb^{3+}/Tm^{3+},[30] Yb^{3+}/Pr^{3+},[31], Yb^{3+}/Mo^{3+}, and Yb^{3+}/Re^{4+}.[32] However, for broadband NIR excitation the Yb^{3+} ion is unsuitable because of its spectrally narrow NIR absorption. Other studies have used the d^3 intraconfigurational, i.e., ligand-field independent transitions of Mo^{3+} and Re^{4+} to sensitize Tm^{3+} upconversion,[33,34] and an analogous approach has been chosen with Os^{4+} as a sensitizer for Er^{3+} upconversion luminescence.[35] However, in all these cases the sensitizers are sharp-line NIR absorbers and thus similar to Yb^{3+}. In our present study we use for the first time a broad spin-allowed ligand-field-dependent d−d absorption located in the NIR to sensitize vis upconversion luminescence.

Our system is V^{3+} and Mo^{3+} codoped Cs_2NaYCl_6. The trivalent dopant ions replace Y^{3+} and are thus in octahedral chloro-coordination. V^{3+} and Mo^{3+} have a $3d^2$ and $4d^3$ electronic configuration, respectively. Figure 1 shows energy level diagrams for octahedrally coordinated d^2 (a) and d^3 (b) ions.[36,37] In the Cs_2NaYCl_6 host VCl_6^{3-} has broad d−d absorptions in the NIR and green spectral regions due to $^3T_{1g} \rightarrow {}^3T_{2g}$ and $^3T_{1g} \rightarrow {}^3T_{1g}$ transitions, respectively, but it is transparent in the red.[38] $MoCl_6^{3-}$ has been shown to convert NIR energy into red light output at cryogenic temperatures.[25,39] It has only two metastable excited states, ^2E_g and $^2T_{2g}$, and thus its upconversion behavior can be understood within a simple "pseudo-three-level" picture, which greatly facilitates the theoretical analysis. The fact that both dopant ions are trivalent allows us to vary the relative V^{3+} and Mo^{3+} dopant concentrations in Cs_2NaYCl_6 to a considerable extent.

II. Experimental Section

A. Crystal Growth and Handling. Cs_2NaYCl_6 single crystals doped with V^{3+} and Mo^{3+} were grown from the melt by the Bridgeman technique using appropriate stoichiometric amounts of CsCl, NaCl (both Merck suprapur), YCl_3 (prepared from 99.999% pure Y_2O_3 from Fluka), VCl_3 (Atomergic Chemetals 99%), and $MoCl_3$ (Cerac 99.5%). The effective furnace temperature was 850 °C, and the pulling rate was 0.01 mm/min.[40] Crystals of good optical quality with 5 mm diameter and up to 20 mm length were obtained. The effective V^{3+} and Mo^{3+} dopant concentrations in the crystals were determined by induction coupled plasma spectroscopy (ICPS), for which a small part of the sample was dissolved, sprayed into an argon plasma, and the vanadium/molybdenum emission was detected. Table 1 summarizes all crystals used for this study. The abbreviation codes which are used for these crystals throughout this paper are also listed in Table 1. All samples and precursors were handled under inert nitrogen and helium atmospheres. For absorption and lamp excitation (upconversion) measurements samples with plane-parallel polished surfaces were enclosed in copper cells. For luminescence experiments the crystals were sealed in quartz ampules under a partial pressure of helium, which serves both as an inert gas and as a heat transmitter.

TABLE 1: Summary and Abbreviation Codes of All Crystals Used in This Study

abbrev. code	sample	spectroscopic experiments[a]
(3.0/0)	3% V^{3+}:Cs_2NaYCl_6	absorption
(0.6/0)	0.6% V^{3+}:Cs_2NaYCl_6	luminescence, UC, lifetimes
(0.1/0.3)	0.1% V^{3+}:0.3% Mo^{3+}:Cs_2NaYCl_6	luminescence, UC, lifetimes
(0.2/4.3)	0.2% V^{3+}:4.3% Mo^{3+}:Cs_2NaYCl_6	luminescence, UC, ifetimes
(0.8/0.3)	0.8% V^{3+}:0.3% Mo^{3+}:Cs_2NaYCl_6	luminescence, UC, lifetimes
(0/0.3)	0.3% Mo^{3+}:Cs_2NaYCl_6	luminescence, UC, lifetimes
(0/7.5)	7.5% Mo^{3+}:Cs_2NaYCl_6	absorption

[a] The last column indicates which spectroscopic experiments have been performed with the various crystals. UC denotes upconversion.

B. Spectroscopic Measurements. Absorption spectra were measured on a Cary 5e (Varian) spectrometer. Sample cooling was achieved with a closed-cycle helium cryostat (Air Products Displex). Continuous-wave (cw) luminescence experiments were performed using various excitation sources: An argon laser (Spectra-Physics 2060−20 SA) pumped Ti^{3+}:sapphire laser (Spectra-Physics 3900 S) for V^{3+} $^3T_{2g}$ and Mo^{3+} ^2E_g, $^2T_{1g}$ excitation, the 514.5 nm (19436 cm^{-1}) line of an argon laser for V^{3+} $^3T_{1g}$ excitation, and the 676.4 nm (14784 cm^{-1}) line of a krypton laser (Coherent CR 550 K) for Mo^{3+} $^2T_{2g}$ excitation. The sample luminescence was dispersed by a 0.75 m single monochromator equipped with a 750 nm blazed (600 grooves/mm) grating. Detection of V^{3+} $^1T_{2g} \rightarrow {}^3T_{1g}$ and Mo^{3+} $^2E_g \rightarrow {}^4A_{2g}$ luminescence occurred with a liquid nitrogen cooled germanium detector (ADC 403L) connected to a lock-in amplifier (Stanford Research 830). Mo^{3+} $^2T_{2g} \rightarrow {}^4A_{2g}$ luminescence was detected with a cooled photomultiplier tube (RCA C31034) connected to a photon counting system (Stanford Research 400).

For the lifetime measurements the laser beams of the above cw excitation sources were passed through an acousto-optical modulator (Coherent 305) connected to a function generator (Stanford Research DS345) to obtain square-wave excitation pulses. Detection of the NIR luminescence decays occurred with a fast-response germanium detector (ADC 403HS, 2 μs response), and the transients were recorded on an oscilloscope (Tektronix TDS 540A). Mo^{3+} $^2T_{2g}$ decays were measured using the RCA C31034 PMT connected to a multichannel scaler (Stanford Research 430).

Upconversion excitation measurements were performed using one or two tunable Ti^{3+}:sapphire lasers (see above). Their output wavelength was controlled using a step-motor-driven three-component birefringent filter, and the laser wavelength was monitored using a wave-meter (Burleigh WA 2100S). The wavelength dependence of the laser power was always measured in parallel to the excitation spectra using a power meter (Coherent Labmaster E). Typical excitation powers used were on the order of 20−300 mW, and the laser beam with a diameter of roughly 1 mm was focused onto the crystals with a 53 mm

TABLE 2: The 15 K V^{3+} $^1T_{2g} \rightarrow {}^3T_{1g}$ (I_V^{Vexc}) versus Mo^{3+} $^2E_g \rightarrow {}^4A_{2g}$ ($I_{Mo}^{Vexc.}$) Luminescence Photon Ratios[a] Observed in Various V^{3+} and Mo^{3+} Codoped Cs_2NaYCl_6 Crystals after V^{3+} $^3T_{2g}$ Excitation at 11000 cm^{-1},[b] the Calculated $I_{Mo}^{Vexc}/(I_{Mo}^{Vexc} + I_V^{Vexc})$ Photon Ratios,[c] the Calculated (see Section IV.B) Ratio of the V^{3+} $^1T_{2g}$ versus Mo^{3+} ^2E_g Steady State Population Densities after Continuous-Wave Laser Excitation into V^{3+} $^3T_{2g}$ at 11000 cm^{-1} [d]

code	crystal	$I_V^{Vexc}I_{Mo}^{Vexc}$	$I_{Mo}^{Vexc}/(I_{Mo}^{Vexc.}+I_V^{Vexc.})$	$N_V^{Vexc}:N_{Mo}^{Vexc}$
(0.1/0.3)	$0.1\%V^{3+}:0.3\%Mo^{3+}:Cs_2NaYCl_6$	6:1	1/7	1.8
(0.2/4.3)	$0.2\%V^{3+}:4.3\%Mo^{3+}:Cs_2NaYCl_6$	1:1	1/2	0.3
(0.8/0.3)	$0.8\%V^{3+}:0.3\%Mo^{3+}:Cs_2NaYCl_6$	3:1	1/4	0.9

[a] The ratio for the (0.1/0.3) sample was extracted from part c of Figure 3; the ratios for the (0.2/4.3) and (0.8/0.3) samples were obtained from analogous experiments (spectra not shown). [b] Third column. [c] Fourth column. [d] Fifth column.

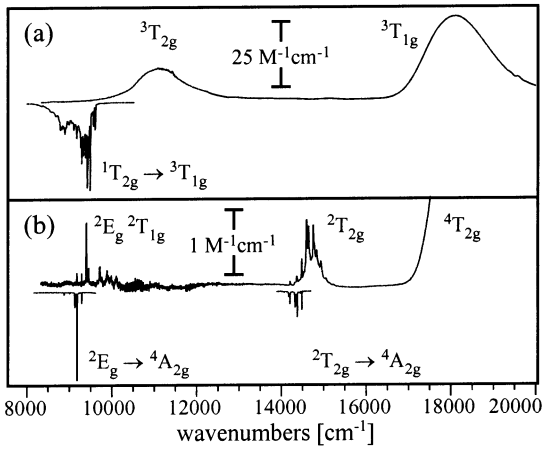

Figure 2. (a) 15 K survey absorption spectrum of 3% $V^{3+}:Cs_2NaYCl_6$ and 15 K luminescence spectrum of 0.6% $V^{3+}:Cs_2NaYCl_6$ obtained after excitation at 19436 cm^{-1}. (b) 15 K survey absorption spectrum of 7.5% $Mo^{3+}:Cs_2NaYCl_6$ and 15 K luminescence spectrum of 0.3% $Mo^{3+}:Cs_2NaYCl_6$ obtained after excitation at 14784 cm^{-1}.

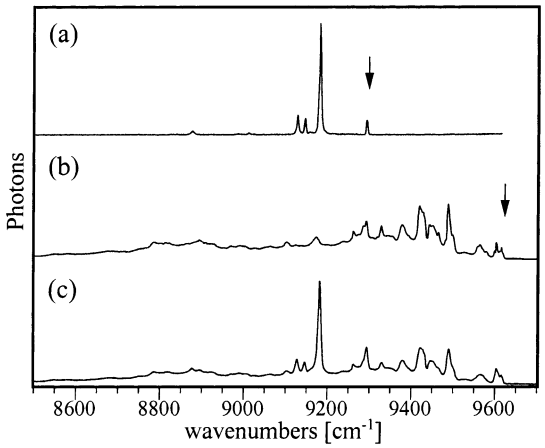

Figure 3. 15 K near-infrared luminescence spectra of (a) 0.3% $Mo^{3+}:Cs_2NaYCl_6$ excited at 9712 cm^{-1}, (b) 0.6% $V^{3+}:Cs_2NaYCl_6$ excited at 11000 cm^{-1}, and (c) 0.1% V^{3+} and 0.3% Mo^{3+} codoped Cs_2NaYCl_6 excited at 11000 cm^{-1}. The arrows in (a) and (b) indicate the energies of the electronic Mo^{3+} ^2E_g and V^{3+} $^1T_{2g}$ origins.

focal length lens. Thus, laser power densities of up to 10 kW/cm^2 are achieved. [41] Mo^{3+} upconversion luminescence was dispersed by a 0.85 m double monochromator equipped with 500 nm blazed (1200 grooves/mm) gratings and detected with a PMT as described above. The Mo^{3+} $^2T_{2g} \rightarrow {}^4A_{2g}$ ("vis") versus Mo^{3+} $^2E_g \rightarrow {}^4A_{2g}$ and V^{3+} $^1T_{2g} \rightarrow {}^3T_{1g}$ ("NIR") photon ratios after near-infrared laser excitation were measured with the same setup using a dry ice cooled lead sulfide detector (Hamamatsu P3337) connected to a lock-in amplifier (see above).

Broadband near-infrared excitation occurred with the focused output from a 70-W tungsten lamp passing through three long-pass filters (Baltzers RG 780). Both samples used were cut and polished circular crystal plates of 5 mm diameter and 3 mm thickness with good optical quality. Detection of the upconversion luminescence occurred from the crystal faces on the opposite side of the excitation source with the system described above. In all luminescence experiments sample cooling was achieved with a helium gas flow technique using home-built quartz flow tubes or a home-built metal helium flow cryostat equipped with quartz windows. All luminescence spectra were corrected for the wavelength dependence of the detection system sensitivity, and they were converted to photon counts versus wavenumber using the procedure described in ref 42. All upconversion excitation spectra were corrected for the wavelength dependence of the excitation laser power P by dividing the raw data by P^2.

III. Results

In the following we use the abbreviation code defined in Table 1 to designate the various samples. Figure 2 shows 15 K survey absorption and luminescence spectra of (a) $V^{3+}:Cs_2NaYCl_6$ and (b) $Mo^{3+}:Cs_2NaYCl_6$ (lower half) in the 7000−20000 cm^{-1} spectral range. The V^{3+} concentrations were 3% and 0.6% for absorption and luminescence, respectively, and the Mo^{3+} concentrations 7.5% and 0.3%, respectively. The luminescence spectra are displayed upside down, and they were obtained after V^{3+} $^3T_{1g}$ excitation at 19436 cm^{-1} and Mo^{3+} $^2T_{2g}$ excitation at 14784 cm^{-1}. The (0.6/0) crystal exhibits one richly structured luminescence band located in the near-infrared (see Table 1 for abbreviation code). Two emission bands, one in the near-infrared and one in the visible spectral region, are observed from the (0/0.3) crystal at 15 K.

Figure 3 shows 15 K high-resolution near-infrared luminescence spectra of (a) (0/0.3) excited at 9712 cm^{-1}, (b) (0.6/0) excited at 11000 cm^{-1}, and (c) (0.1/0.3) excited at 11000 cm^{-1}. The luminescence spectrum of the purely Mo^{3+} doped sample (a) essentially consists of four sharp lines with the most prominent one located at 9180 cm^{-1}. The V^{3+} luminescence spectrum (b) is comprised of numerous lines resulting in a significantly broader overall band shape. The 15 K luminescence spectrum of the (0.1/0.3) crystal (c) was obtained after V^{3+} excitation and is essentially a superposition of (a) and (b). Its quantitative evaluation yields a $V^{3+}:Mo^{3+}$ photon ratio $I_V^{Vexc.}:I_{Mo}^{Vexc}$ of 6:1 for (0.1/0.3). As indicated in the third column of Table 2, for the (0.2/4.3) and (0.8/0.3) samples $I_V^{Vex.}:I_{Mo}^{Vexc}$ ratios of 1:1 and 3:1, respectively, are obtained.

The third column in Table 3 lists the 15 K V^{3+} $^1T_{2g}$ lifetimes in a purely V^{3+} doped and three $V^{3+}:Mo^{3+}$ codoped Cs_2NaYCl_6 crystals. The respective transients were obtained after square-wave pulsed excitation at 11000 cm^{-1}, and detection occurred at 9480 cm^{-1}. All decays are essentially single exponential (data not shown). Table 3 shows that the presence of Mo^{3+} generally leads to a shortening of the V^{3+} $^1T_{2g}$ lifetime, but this effect is less dramatic for the (0.1/0.3) and (0.8/0.3) crystals than for

TABLE 3: The V^{3+} $^1T_{2g} \rightarrow {}^3T_{1g}$ Luminescence Decay Time $\tau_{tot,V}$ Detected at 9480 cm^{-1} [a] and Its Inverse $k_{tot,V}$,[b] and V^{3+} $^1T_{2g} \rightarrow Mo^{3+}$ ^2E_g, $^2T_{1g}$ Energy Transfer Rate Constants k_{ET}[c] and Inherent V^{3+} $^1T_{2g}$ Decay Rate Constant k_V at 15 K[d]

code	crystal	$\tau_{tot,V}$ [ms]	$k_{tot,V}$ [s^{-1}]	k_{ET} [s^{-1}]	k_V [s^{-1}]
(0/0.6)	$0.6\%V^{3+}:Cs_2NaYCl_6$	17.2	58		58
(0.1/0.3)	$0.1\%V^{3+}:0.3\%Mo^{3+}:Cs_2NaYCl_6$	16.4	61	9	52
(0.2/4.3)	$0.2\%V^{3+}:4.3\%Mo^{3+}:Cs_2NaYCl_6$	10.0	100	50	50
(0.8/0.3)	$0.8\%V^{3+}:0.3\%Mo^{3+}:Cs_2NaYCl_6$	14.7	68	17	51

[a] Third column. [b] Fourth column. [c] Fifth column. [d] Sixth column.

TABLE 4: 15 K Mo^{3+} ^2E_g and $^2T_{2g}$ Lifetimes in Various Crystals

abbrev. code	crystal	$\tau(^2E_g)$ [ms]	$\tau(^2T_{2g})$ [μs]
(0/0.3)	$0.3\%\ Mo^{3+}:Cs_2NaYCl_6$	67.5	398
(0.1/0.3)	$0.1\%V^{3+}:0.3\%Mo^{3+}:Cs_2NaYCl_6$	69.4	398
(0.2/4.3)	$0.2\%V^{3+}:4.3\%Mo^{3+}:Cs_2NaYCl_6$	67.2	403
(0.8/0.3)	$0.8\%V^{3+}:0.3\%Mo^{3+}:Cs_2NaYCl_6$	67.0	395

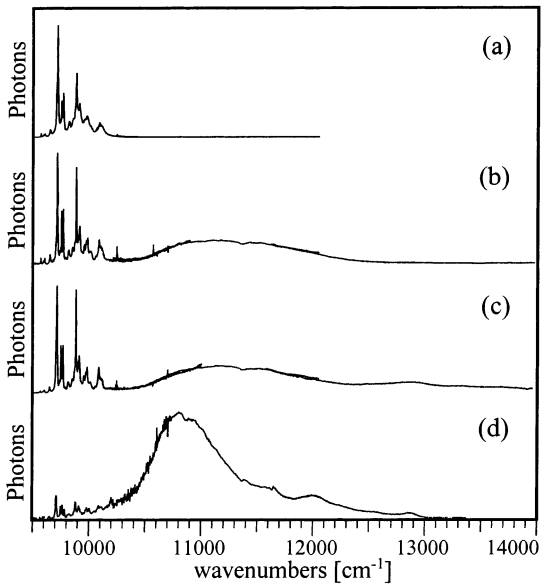

Figure 4. 15 K near-infrared excitation spectra of Mo^{3+} $^2T_{2g} \rightarrow {}^4A_{2g}$ upconversion luminescence detected at 14368 cm^{-1} for (a) 0.3% $Mo^{3+}:Cs_2NaYCl_6$ (0/0.3), (b) 0.1% V^{3+}:0.3% Mo^{3+} (0.1/0.3), (c) 0.2% V^{3+}:4.3% Mo^{3+} (0.2/4.3), and (d) 0.8% V^{3+}:0.3% Mo^{3+} codoped Cs_2NaYCl_6 (0.8/0.3).

(0.2/4.3). The third and fourth columns in Table 4 list 15 K lifetimes of the metastable Mo^{3+} ^2E_g and $^2T_{2g}$ excited states, respectively, for various crystals. Luminescence decays were monitored at 9180 and 14368 cm^{-1}, respectively. Excitation occurred with square-wave excitation pulses at 9712 and 14784 cm^{-1}, respectively. All decays are essentially single exponential (data not shown). Both Mo^{3+} excited-state lifetimes are unaffected by the presence of V^{3+}. Figure 4 exhibits 15 K NIR excitation spectra of vis Mo^{3+} $^2T_{2g} \rightarrow {}^4A_{2g}$ luminescence detected at 14368 cm^{-1} for (a) (0/0.3), (b) (0.1/0.3), (c) (0.2/4.3), and (d) (0.8/0.3). The 15 K upconversion excitation spectrum of the purely Mo^{3+} doped crystal (a) consists of several sharp lines between 9500 and 10200 cm^{-1}. These lines coincide with the Mo^{3+} $^2T_{1g}$ NIR absorption lines in Figure 2. Excitation at higher energies does not induce any upconversion luminescence in this sample. In contrast, the spectra of the V^{3+}:Mo^{3+} codoped samples (b−d) contain an additional broad band extending from roughly 10000 to about 12500 cm^{-1}. The broadband versus sharp-line photon ratio in the upconversion excitation spectra in Figure 4 depends on the relative V^{3+} and Mo^{3+} dopant concentrations. It is about 4:1 in both (0.1/0.3) (b) and (0.2/4.3) (c), and roughly 60:1 in (0.8/0.3) (d). In addition, there is a significant difference in the shapes of the broad excitation bands in (b)/(c) on one hand and (d) on the other hand. Whereas the former have their maximum around 11200 cm^{-1}, i.e., coincident with the V^{3+} NIR absorption band maximum in Figure 2, the upconversion excitation band in (d) is narrower and maximizes around 10800 cm^{-1}. Figure 5a shows the near-infrared part of the 15 K absorption spectrum of (3.0/0) from Figure 2 on an enlarged energy scale. The dashed line in part b of Figure 5 is an extract from the 15 K ground-state absorption (GSA) spectrum of (0/7.5) shifted down in energy by 9292 cm^{-1}, corresponding to the energy of the metastable Mo^{3+} ^2E_g excited state. It is referred to hereafter as the putative Mo^{3+} $^2E_g \rightarrow {}^4T_{2g}$, $^4T_{1g}$ excited-state absorption (ESA) spectrum. The strong line in part b of Figure 5 is the result of a pump and probe experiment performed with (0/0.3) at 15 K. The pump laser excited Mo^{3+} at 9712 cm^{-1} with an estimated laser power density of about 3.7 kW/cm^2 (see section II.B and ref 41), thus ensuring a significant Mo^{3+} ^2E_g excited-state population. The probe laser was scanned using a power density below 0.05 kW/cm^2, to avoid upconversion by the probe beam alone. The resulting two-color excitation spectrum has a similar shape as the putative Mo^{3+} $^2E_g \rightarrow {}^4T_{2g}$ ESA spectrum between 10400 and 11000 cm^{-1}. Part c of Figure 5 is the calculated product of the spectra a and b, and it is discussed in section IV.C. The

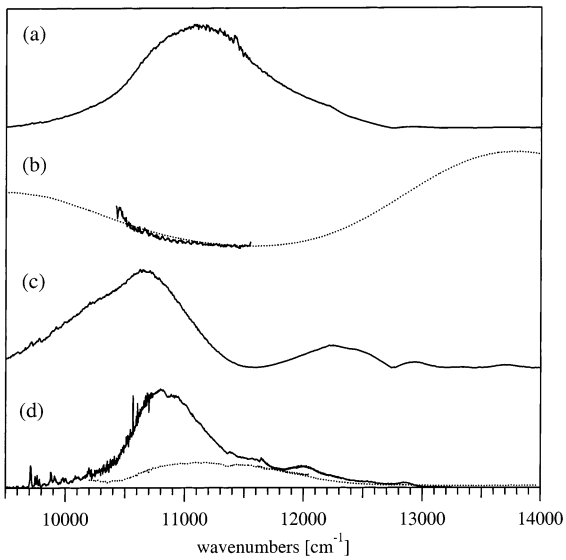

Figure 5. (a) 15 K V^{3+} $^3T_{1g} \rightarrow {}^3T_{2g}$ ground-state absorption (GSA) spectrum of 3% $V^{3+}:Cs_2NaYCl_6$. (b) The dashed line is the putative 15 K Mo^{3+} $^2E_g \rightarrow {}^4T_{2g}$, $^4T_{1g}$ excited-state absorption (ESA) spectrum, and it was obtained by shifting the Mo^{3+} $^4A_{2g} \rightarrow {}^4T_{2g}$, $^4T_{1g}$ GSA spectrum of 7.5% $Mo^{3+}:Cs_2NaYCl_6$ down in energy by 9292 cm^{-1}, which corresponds to the energy of the intermediate ^2E_g excited state. The solid line between 10400 and 11600 cm^{-1} is the 15 K Mo^{3+} $^2E_g \rightarrow {}^4T_{2g}$ excited-state excitation spectrum of 0.3% $Mo^{3+}:Cs_2NaYCl_6$. The trace in (c) is the calculated product of the GSA and ESA spectra in (a) and (b), respectively. (d) The solid line is the same as in Figure 4d: 15 K excitation spectrum of Mo^{3+} $^2T_{2g} \rightarrow {}^4A_{2g}$ upconversion luminescence in 0.8% V^{3+}:0.3% $Mo^{3+}:Cs_2NaYCl_6$, detected at 14368 cm^{-1}. The dashed line is the same as that in Figure 4b.

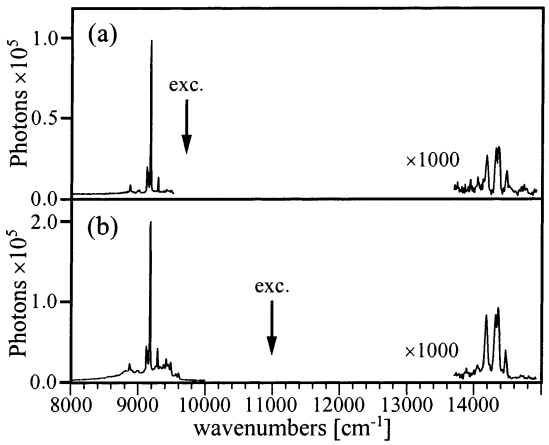

Figure 6. 15 K luminescence spectra of 0.8% V^{3+}:0.3% Mo^{3+}:Cs_2NaYCl_6 (0.8/0.3), obtained after excitation with equal excitation densities at (a) 9721 cm^{-1} and (b) 11000 cm^{-1}, see arrows. Note the different *y*-scales in (a) and (b).

TABLE 5: Relative Photon Counts of Visible Mo^{3+} $^2T_{2g} \rightarrow {}^4A_{2g}$ (vis) and near-Infrared Mo^{3+} $^2E_g \rightarrow {}^4A_{2g}$ Plus V^{3+} $^1T_{2g} \rightarrow {}^3T_{1g}$ Luminescence (NIR) in Mo^{3+} Doped and Various V^{3+}:Mo^{3+} Codoped Cs_2NaYCl_6 Crystals at 15 K after Direct Mo^{3+} Excitation at 9712 cm^{-1} and after V^{3+} Excitation at 11000 cm^{-1} [a]

abbrev. code	crystal	vis:NIR, Mo^{3+} exc	vis:NIR, V^{3+} exc
(0/0.3)	0.3%Mo^{3+}:Cs_2NaYCl_6	1.0×10^{-3}	
(0.1/0.3)	0.1%V^{3+}:0.3%Mo^{3+}:Cs_2NaYCl_6	0.9×10^{-3}	0.1×10^{-3}
(0.2/4.3)	0.2%V^{3+}:4.3%Mo^{3+}:Cs_2NaYCl_6	2.0×10^{-3}	0.5×10^{-3}
(0.8/0.3)	0.8%V^{3+}:0.3%Mo^{3+}:Cs_2NaYCl_6	1.4×10^{-3}	0.9×10^{-3}

[a] In all experiments an identical laser power density was used; see section II for details.

solid line in part d of Figure 5 is the 15 K upconversion excitation spectrum of (0.8/0.3) from part d of Figure 4.

Figure 6 shows the 15 K 8000−15000 cm^{-1} survey luminescence spectra of (0.8/0.3) obtained after (a) Mo^{3+} excitation at 9712 cm^{-1} and (b) V^{3+} excitation at 11000 cm^{-1}. Both spectra were obtained using a laser power density of roughly 10 kW/cm^2 (see above). Note that in both spectra the luminescence lines between 13700 and 14900 cm^{-1} are scaled up by a factor of 1000. The ratio of the total amount of photons emitted at 15 K in the visible and in the near-infrared (vis:NIR) extracted from these spectra is 1.4×10^{-3} for Mo^{3+} excitation and 0.9×10^{-3} for V^{3+} excitation, see Table 5. As shown in Table 5, in all V^{3+}:Mo^{3+} codoped crystals the vis:NIR ratio is higher for direct Mo^{3+} than for V^{3+} monochromatic laser excitation, and in all crystals studied here, the vis:NIR ratio is on the order of $10^{-3}-10^{-4}$.

Figure 7 presents 15 K upconversion luminescence spectra of (a) (0.8/0.3) and (b) (0/0.3) obtained after broadband NIR (lamp) excitation as described in section IIB. Spectrum (a) is identical to the Mo^{3+} vis luminescence spectra presented in Figures 2 and 6. In the case of the purely Mo^{3+} doped crystal (b), no upconversion luminescence can be detected under these experimental conditions.

IV. Analysis and Discussion

A. Absorption and Luminescence Properties of V^{3+}:Cs_2NaYCl_6 and Mo^{3+}:Cs_2NaYCl_6. The absorption and luminescence properties of V^{3+} doped Cs_2NaYCl_6 have been described and analyzed in detail in refs 38 and 43. Two broad absorption bands with oscillator strengths f of 6×10^{-5} and 20

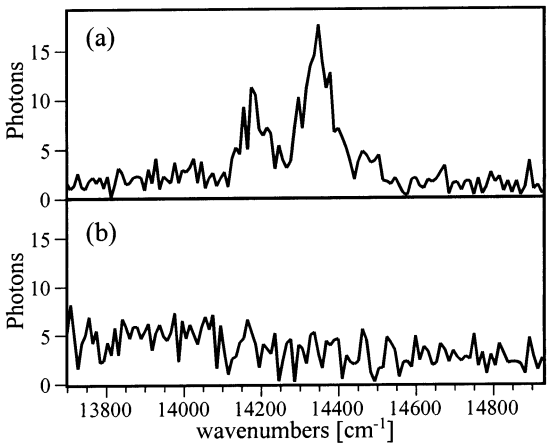

Figure 7. (a) 15 K Mo^{3+} $^2T_{2g} \rightarrow {}^4A_{2g}$ upconversion luminescence spectrum of 0.8% V^{3+}:0.3% Mo^{3+}:Cs_2NaYCl_6 (0.8/0.3), obtained after excitation with the broadband near-infrared output of a tungsten lamp below 12500 cm^{-1}. (b) Result of the same experiment with 0.3% Mo^{3+}:Cs_2NaYCl_6 (0/0.3).

$\times 10^{-5}$ due to $^3T_{1g} \rightarrow {}^3T_{2g}$ and $^3T_{1g} \rightarrow {}^3T_{1g}$ transitions, respectively, are observed, see part a of Figure 2. The crystal field strength acting on V^{3+} in Cs_2NaYCl_6 is illustrated by the dashed vertical line at $10Dq/B = 18.6$ in part a of Figure 1. The lowest energetic excited state of V^{3+} is $^1T_{2g}$, part a of Figure 1, and thus the 15 K luminescence in part a of Figure 2 is due to the spin-forbidden V^{3+} $^1T_{2g} \rightarrow {}^3T_{1g}$ transition. Unlike for the d^2 ion Ti^{2+} in hexa-chloro coordination,[44−46] to date no emission from a higher excited state has been reported for VCl_6^{3-}.

The absorption and luminescence properties of Mo^{3+} doped Cs_2NaYCl_6 have been reported and discussed in refs 25 and 39. Up to 17000 cm^{-1} only sharp and comparatively weak ($f \approx 10^{-7}$) Mo^{3+} absorption features are observed, see part b of Figure 2. This is because in Mo^{3+}:Cs_2NaYCl_6 $10Dq/B = 38.6$,[47] see the dashed vertical line in part b of Figure 1. Thus the three lowest energetic electronic absorptions in part b of Figure 2 are due to $^4A_{2g} \rightarrow {}^2E_g/{}^2T_{1g}$ (9000−10000 cm^{-1}) and $^4A_{2g} \rightarrow {}^2T_{2g}$ (14500 cm^{-1}) spin-flip transitions.[48] Transitions from the $^4A_{2g}$ ground state to these excited states all occur within the t_{2g}^3 electron configuration, and consequently their distortions with respect to $^4A_{2g}$ and with respect to each other are small. This fact greatly influences the luminescence behavior of Mo^{3+}:Cs_2NaYCl_6 in that nonradiative relaxation processes from both ^2E_g and $^2T_{2g}$ are largely suppressed at cryogenic temperatures.[39] Thus the situation here is similar to the trivalent lanthanides, where f−f excited state distortions are similarly low.[15] In this so-called weak coupling limit, the competition between radiative and nonradiative deactivation processes is governed by the energetic separations between the individual electronic states. The so-called energy gap law is well established to estimate multiphonon relaxation rate constants k_{mp} in lanthanide systems:[49]

$$k_{mp} = \beta \exp(-\alpha p) \qquad (1)$$

where α and β are parameters characteristic of the material and $p = \Delta E/(\hbar\omega)$ is the number of phonons of energy $\hbar\omega$ required to bridge the electronic energy gap ΔE. Usually the highest energy vibrational mode is relevant.[50] As soon as $p > 5$, luminescence usually becomes dominant over multiphonon relaxation.[51,52] This is the case for the $^2E_g - {}^4A_{2g}$ and $^2T_{2g} - {}^2T_{1g}$ energy gaps in Mo^{3+}:Cs_2NaYCl_6, and from this viewpoint it is not surprising that at 15 K ^2E_g and $^2T_{2g}$ depopulation occurs

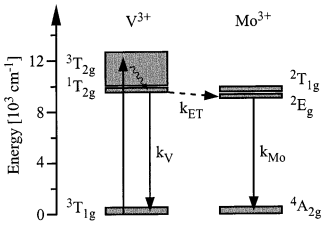

Figure 8. Schematic illustration of photophysical processes in V^{3+}, Mo^{3+} codoped Cs_2NaYCl_6 including the energy levels of V^{3+} (left) and Mo^{3+} (right) between 0 and 14000 cm^{-1}. The solid upward and downward arrows represent absorption and luminescence processes, respectively. The wavy and the dashed arrows represent multiphonon relaxation and energy transfer processes, respectively.

entirely radiatively.[39] This leads to the $^2E_g \rightarrow {}^4A_{2g}$ and $^2T_{2g} \rightarrow {}^4A_{2g}$ luminescence transitions shown in part b of Figure 2. Additional $^2T_{2g} \rightarrow {}^2E_g$, $^2T_{1g}$ inter-excited-state luminescence is also observed at ca. 5000 cm^{-1}, but not shown.[19] With its two metastable excited states the Mo^{3+}:Cs_2NaYCl_6 system is capable to exhibit upconversion phenomena.[25,39] However, this is only possible below 175 K. Above this temperature, the Mo^{3+} luminescences are quenched.[39,53]

B. Energy Transfer Processes between V^{3+} and Mo^{3+} in the Codoped Cs_2NaYCl_6 Crystals. *i. $V^{3+1}T_{2g} \rightarrow Mo^{3+2}E_g$, $^2T_{1g}$ Energy Transfer in the near-Infrared.* The observation of both V^{3+} $^1T_{2g} \rightarrow {}^3T_{1g}$ and Mo^{3+} $^2E_g \rightarrow {}^4A_{2g}$ luminescence after 15 K V^{3+} $^3T_{2g}$ excitation at 11000 cm^{-1} in the (0.1/0.3) crystal, part c of Figure 3, is direct evidence for a partial $V^{3+} \rightarrow Mo^{3+}$ energy transfer process. This is confirmed by the observed shortening of the 15 K V^{3+} $^1T_{2g}$ lifetime $\tau_{tot,V}$ from 17.2 to 16.4 μs in the presence of Mo^{3+}, see Table 3. Figure 8 shows an energy level scheme including the V^{3+} and Mo^{3+} states below 14000 cm^{-1}. It illustrates that after V^{3+} $^3T_{2g}$ excitation (upward arrow) nonradiative relaxation to $^1T_{2g}$ occurs (wavy arrow), from which V^{3+} $^1T_{2g} \rightarrow {}^3T_{1g}$ luminescence (left downward arrow) is in competition with V^{3+} $^1T_{2g} \rightarrow Mo^{3+}$ ^2E_g, $^2T_{1g}$ energy transfer (dashed arrow) and subsequent Mo^{3+} $^2E_g \rightarrow {}^4A_{2g}$ luminescence (right downward arrow). This competition is governed by the relative magnitudes of the $V^{3+} \rightarrow Mo^{3+}$ energy transfer rate constant k_{ET} and the V^{3+} $^1T_{2g} \rightarrow {}^3T_{1g}$ luminescence decay rate constant k_V. At 15 K there is no multiphonon relaxation from either the V^{3+} $^1T_{2g}$ or the Mo^{3+} ^2E_g excited state. Consequently, k_{ET} can be calculated using

$$k_{ET} = k_{tot,V}\frac{I_{Mo}^{Vexc.}}{I_{Mo}^{Vexc.} + I_V^{Vexc}} \qquad (2)$$

where $k_{tot,V}$ is the total V^{3+} $^1T_{2g}$ decay rate constant, i.e., the inverse of the experimental 15 K lifetime $\tau_{tot,\,V}$, see fourth column of Table 3. $I_{Mo}^{Vexc.}/(I_{Mo}^{Vexc.} + I_V^{Vexc})$ is the photon ratio of Mo^{3+} $^2E_g \rightarrow {}^4A_{2g}$ versus Mo^{3+} $^2E_g \rightarrow {}^4A_{2g}$ plus V^{3+} $^1T_{2g} \rightarrow {}^3T_{1g}$ NIR luminescence after V^{3+} $^3T_{2g}$ excitation at 15 K, and it is experimentally accessible from luminescence spectra such as the one presented in part c of Figure 3. The photon ratios for all three codoped crystals are listed in the fourth column of Table 2. From this we calculate the V^{3+} $^1T_{2g} \rightarrow Mo^{3+}$ ^2E_g, $^2T_{1g}$ energy transfer rate constants k_{ET} listed in the fifth column of Table 3. k_{ET} increases along the crystal series (0.1/0.3) < (0.8/0.3) < (0.2/4.3). Previous studies on rare earth and transition metal doped elpasolite systems revealed energy transfer rate constants up to the order of 10^3 s^{-1}.[39,54] Thus, our k_{ET} values, which are on the order of 10 s^{-1}, are rather low. We attribute this to the low V^{3+} and Mo^{3+} dopant concentrations and a small spectral overlap integral. Table 3 shows that when going from crystal (0.1/0.3) to crystal (0.2/4.3) the increase in k_{ET} is bigger than when going from crystal (0.1/0.3) to (0.8/0.3). In other words, an increase in the Mo^{3+} concentration is more effective in increasing k_{ET} than an increase in the V^{3+} concentration. From this we conclude that $^1T_{2g}$ energy migration among the V^{3+} ions is relatively inefficient. This is not unexpected because less than 0.1% of the total V^{3+} $^1T_{2g} \rightarrow {}^3T_{1g}$ luminescence intensity lies in the electronic origin. Consequently, the spectral overlap integral for V^{3+} $^1T_{2g} \rightarrow V^{3+}$ $^1T_{2g}$ energy transfer is below 10^{-6} at 15 K, and thus about 3 orders of magnitude smaller than for V^{3+} $^1T_{2g} \rightarrow Mo^{3+}$ ^2E_g, $^2T_{1g}$.

The V^{3+} $^1T_{2g} \rightarrow {}^3T_{1g}$ versus Mo^{3+} $^2E_g \rightarrow {}^4A_{2g}$ photon ratio after 15 K V^{3+} $^3T_{2g}$ excitation $I_V^{Vexc.}$:$I_{Mo}^{Vexc.}$, part c of Figure 3, is determined by the relative decay rates of V^{3+} $^1T_{2g}$ and Mo^{3+} ^2E_g. These rates are the products of the respective decay rate constants k_i and population densities N_i:

$$\frac{I_V^{Vexc}}{I_{Mo}^{Vexc}} = \frac{k_V N_V^{Vexc}}{k_{Mo} N_{Mo}^{Vexc}} \qquad (3)$$

For all three codoped crystals $I_V^{Vexc.}$:$I_{Mo}^{Vexc.}$ ratios are given in Table 2, and k_V and k_{Mo} are listed in Tables 3 and 4, respectively. Thus, eq 3 can be used to calculate the relative steady-state population densities N_V^{Vexc}:N_{Mo}^{Vexc} of the metastable V^{3+} $^1T_{2g}$ and Mo^{3+} ^2E_g states. The ratio k_V:k_{Mo} is roughly 3.4:1 for all three samples. Consequently, since I_V^{Vexc}:$I_{Mo}^{Vexc.}$ is highest in (0.1/0.3), N_V^{Vexc}:N_{Mo}^{Vexc} is highest in this system, see last column in Table 2. However, in all three codoped crystals 15 K continuous-wave V^{3+} $^3T_{2g}$ excitation leads to V^{3+} $^1T_{2g}$ and Mo^{3+} ^2E_g steady-state populations of comparable magnitudes.

ii. Mo^{3+} $^2T_{2g} \rightarrow V^{3+}$ back-Transfer in the Visible. One of the main difficulties in the search for systems where a broadband absorber is combined with an upconversion ion is the potential quenching of the upconversion luminescence by the broadband absorber. In Mo^{3+}:Cs_2NaYCl_6 at 15 K $^2T_{2g} \rightarrow {}^4A_{2g}$ higher excited-state luminescence occurs between 14000 and 14500 cm^{-1}, see part b of Figure 2, and additionally there is $^2T_{2g} \rightarrow {}^2T_{1g}$, ^2E_g inter-excited-state luminescence between 4300 and 5100 cm^{-1} (data not shown).[19] In neither of these two spectral regions is there any significant absorption from the ground state of V^{3+}:Cs_2NaYCl_6 at 15 K, see part a of Figure 2. This is the reason in V^{3+}:Mo^{3+} codoped Cs_2NaYCl_6 at 15 K $^2T_{2g}$ depopulation is fully radiative like in the purely Mo^{3+} doped system: In all three codoped crystals the 15 K Mo^{3+} $^2T_{2g}$ lifetime is around 400 μs, Table 4, and thus essentially identical to the respective value for 0.3% Mo^{3+}:Cs_2NaYCl_6. In none of the three codoped crystals is there any V^{3+} $^1T_{2g} \rightarrow {}^3T_{1g}$ luminescence observable after 15 K Mo^{3+} $^2T_{2g}$ excitation at 14784 cm^{-1}, and we conclude that at 15 K there is no Mo^{3+} $^2T_{2g} \rightarrow V^{3+}$ back-transfer.

C. Upconversion. *i. Excitation Wavelength Dependence and Mechanisms.* It has been demonstrated that in 2.5% Mo^{3+}:Cs_2NaYCl_6 upconversion at 15 K occurs by two competing mechanisms.[25,39] We assume that direct Mo^{3+} excitation of our V^{3+}:Mo^{3+} codoped systems leads to upconversion via the same mechanisms. The 15 K upconversion excitation spectra of the codoped crystals, parts b−d of Figure 4, show that in these systems 15 K Mo^{3+} upconversion luminescence is also induced after excitation between 10000 and 12500 cm^{-1}, i.e., coincident with the V^{3+} $^3T_{1g} \rightarrow {}^3T_{2g}$ absorption band in part a of Figure 2. This is a direct proof that V^{3+} can be used to sensitize 15 K Mo^{3+} upconversion luminescence in Cs_2NaYCl_6. There are three candidate mechanisms which may account for upconversion in our V^{3+}, Mo^{3+} codoped systems, and they are schematically

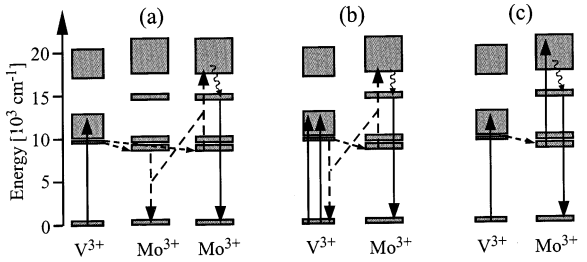

Figure 9. Schematic representations of the possible upconversion mechanisms in V^{3+} and Mo^{3+} codoped Cs_2NaYCl_6. The solid upward and downward arrows indicate absorption and luminescence processes, respectively. The wavy and the dashed arrows represent multiphonon relaxation and energy transfer processes, respectively.

illustrated in Figure 9. In the first mechanism a, V^{3+} only acts as a sensitizer which transfers its excitation energy to Mo^{3+} ^2E_g. This is followed by Mo^{3+} energy transfer upconversion (ETU) as described in ref 39. However, this ETU mechanism is inefficient in 2.5% Mo^{3+}:Cs_2NaYCl_6,[39] and thus mechanism 9a cannot be the dominant upconversion mechanism in our V^{3+}, Mo^{3+} codoped systems.

A second candidate mechanism, part b of Figure 9, involves an ETU step between a ^2E_g excited Mo^{3+} and a $^1T_{2g}$ excited V^{3+} ion. The former receives its energy from a V^{3+} sensitizer. Since the 15 K Mo^{3+} ^2E_g lifetime is more than a factor of 3 longer than the 15 K V^{3+} $^1T_{2g}$ lifetime, see Tables 3 and 4, the same V^{3+} ion can consecutively transfer energy to the same Mo^{3+} ion. For statistical reasons such a two-ion process is more probable than a three ion process involving one Mo^{3+} and two V^{3+} ions.

In the third candidate mechanism, part c of Figure 9, V^{3+} $^1T_{2g} \rightarrow {}^3T_{2g}$ ground-state absorption (GSA) is followed by V^{3+} $^1T_{2g} \rightarrow Mo^{3+}$ ^2E_g energy transfer and then a Mo^{3+} $^2E_g \rightarrow {}^4T_{2g}$ excited-state absorption (ESA) step. Mechanisms 9b and 9c are expected to yield fundamentally different upconversion luminescence excitation spectra. The mechanism in part b of Figure 9 involves twice the V^{3+} $^3T_{1g} \rightarrow {}^3T_{2g}$ GSA transition, but the upconversion step itself is nonradiative. Thus one expects an upconversion excitation spectrum resembling the squared V^{3+} $^3T_{2g}$ GSA spectrum.[12,55] Comparing part a of Figure 2 with the spectra in Figure 4, we note that this is the case for the spectra 4b and 4c, but not for spectrum 4d. The mechanism in part c of Figure 9, on the other hand, involves a radiative upconversion step, and we expect an upconversion excitation spectrum resembling the product of the V^{3+} $^3T_{1g} \rightarrow {}^3T_{2g}$ GSA and Mo^{3+} $^2E_g \rightarrow {}^4T_{2g}$ spectra.[12,55] The following analysis shows that this is the case for the excitation spectrum in part d of Figure 4. Part a of Figure 5 shows the 15 K V^{3+} $^3T_{2g}$ GSA spectrum in detail. Part b of Figure 5 shows the putative Mo^{3+} ESA spectrum in the same spectral region (dashed line). The experimental 15 K Mo^{3+} $^2E_g \rightarrow {}^4T_{2g}$ excited-state excitation (ESE) spectrum (strong line in part b of Figure 5) is in good agreement with the putative Mo^{3+} ESA spectrum. This indicates that the band shape of the latter represents an accurate approximation to the band shape of the real Mo^{3+} $^2E_g \rightarrow {}^4T_{2g}$, $^4T_{1g}$ ESA transitions. The spectrum in part c of Figure 5 is the calculated product of the GSA and ESA spectra from parts a and b of Figure 5. This spectrum exhibits a remarkable similarity to the experimental 15 K upconversion excitation spectrum of crystal (0.8/0.3) from part d of Figure 4, which is duplicated in part d of Figure 5 for better comparison (solid line). In particular, the observed decrease between 10800 and 11400 cm^{-1}, where the GSA in part a of Figure 5 has an increase, clearly demonstrates the importance of the Mo^{3+} $^2E_g \rightarrow {}^4T_{2g}$ ESA process. Thus, we conclude that the dominant upconversion mechanisms are 9b for crystals (0.1/0.3) and (0.2/4.3) and for excitation energies below roughly 11100 cm^{-1}, 9c for crystal (0.8/0.3). Since mechanism 9c cannot account for the complete spectrum in part d of Figure 5 (solid trace), we conclude that for excitation energies above 11100 cm^{-1} mechanism 9b is dominant in this sample, too. This GSA/ETU contribution is indicated by the dashed spectrum in Figure 5d, and it corresponds to the 15 K upconversion excitation spectrum of crystal (0.1/0.3), see part b of Figure 4.

In crystals (0.1/0.3) and (0.8/0.3) the Mo^{3+} dopant concentrations are equal. Consequently, the upconversion efficiencies after Mo^{3+} $^2T_{1g}$ excitation are about equal, see below. Thus, from a comparison of the sharp-line to broadband photon ratios in the 15 K upconversion excitation spectra in parts b and d of Figure 4 we estimate that the efficiency of the V^{3+}/Mo^{3+} ETU mechanism in part b of Figure 9 in crystal (0.8/0.3) is about a factor of 6 higher than in crystal (0.1/0.3). For the V^{3+}/Mo^{3+} GSA/ESA mechanism in part c of Figure 9 we estimate that in crystal (0.8/0.3) its efficiency is increased by at least an order of magnitude compared to crystal (0.1/0.3). This GSA/ESA efficiency enhancement is explained as follows: In crystal (0.8/0.3) the V^{3+} dopant concentration is 8 times higher than in crystal (0.1/0.3), i.e., for a given laser wavelength the V^{3+} $^3T_{1g} \rightarrow {}^3T_{2g}$ GSA cross section is a factor of 8 bigger in crystal (0.8/0.3). In addition, in crystal (0.8/0.3) V^{3+} $^1T_{2g} \rightarrow Mo^{3+}$ ^2E_g, $^2T_{1g}$ energy transfer is a factor of 2 more efficient than in crystal (0.1/0.3), see Table 3. Consequently, in crystal (0.8/0.3), a given laser power leads to a Mo^{3+} ^2E_g population density N_{Mo}^{Vexc} which is roughly a factor of 16 higher than in crystal (0.1/0.3). For mechanism 9c the Mo^{3+} $^2E_g \rightarrow {}^4T_{2g}$ ESA rate is proportional to N_{Mo}^{Vexc}, and we therefore expect an enhancement factor of 16 for mechanism 9c in crystal (0.8/0.3) compared to that of crystal (0.1/0.3).

Interestingly the upconversion excitation spectra of crystal (0.1/0.3), part b of Figure 4, and crystal (0.2/4.3), part c of Figure 4, exhibit a striking similarity, in particular regarding the sharp-line versus broadband intensity ratio. This is explained as follows. In (0.2/4.3) the Mo^{3+} dopant concentration is a factor of 14 higher than in (0.1/0.3). In the former, on the other hand, the V^{3+} concentration is a factor of 2 higher and 15 K V^{3+} $^1T_{2g} \rightarrow Mo^{3+}$ ^2E_g energy transfer is a factor of 5.5 more efficient, see Table 3. Consequently, in crystal (0.2/4.3) the Mo^{3+} and V^{3+} upconversion excitation bands are both enhanced by about an order of magnitude relative to crystal (0.1/0.3), and thus the sharp-line versus broadband intensity ratio is similar in the spectra of parts b and c of Figure 4.

ii. Visible to near-Infrared Luminescence Photon Ratios after near-Infrared Excitation. Figure 6 shows that with an estimated near-infrared laser power density of roughly 10 kW/cm^2 a Mo^{3+} $^2T_{2g} \rightarrow {}^4A_{2g}$ vis upconversion to NIR luminescence photon ratio on the order of 1:1000 is obtained for crystal (0.8/0.3) at 15 K, irrespective of whether excitation occurs into Mo^{3+} $^2T_{1g}$ (part a of Figure 6) or V^{3+} $^3T_{2g}$ (part b of Figure 6). In all other Mo^{3+} doped crystals studied here, this vis:NIR luminescence photon ratio is similarly low, see Table 5. Thus, the absolute Mo^{3+} upconversion efficiency is rather modest when compared to other systems,[56−60] and the reasons for this have been discussed in detail previously.[25,39] Briefly, the very low oscillator strength of the spin-forbidden Mo^{3+} $^2E_g \rightarrow {}^4T_{2g}$ ESA transition is disadvantageous for both GSA/ESA and GSA/ETU mechanisms. Additionally, the Mo^{3+} $^2T_{2g}$ emission branching ratio is about 12:1 in favor of Mo^{3+} $^2T_{2g} \rightarrow {}^2E_g$, $^2T_{1g}$ inter-excited-

state luminescence around 5000 cm^{-1} relative to visible $^2T_{2g} \rightarrow {}^4A_{2g}$ luminescence.[39]

In all crystals considered here the vis:NIR luminescence photon ratio is somewhat lower for 11000 cm^{-1} than for 9712 cm^{-1} excitation, see Table 5. As discussed in Sec. IV B, V^{3+} $^1T_{2g} \rightarrow Mo^{3+}$ ^2E_g, $^2T_{1g}$ energy transfer is not quantitative, i.e., after V^{3+} $^3T_{2g}$ excitation there is not only Mo^{3+} $^2E_g \rightarrow {}^4A_{2g}$ but also V^{3+} $^1T_{2g} \rightarrow {}^3T_{1g}$ near-infrared luminescence, compare parts a and b of Figure 6. In addition, for a given laser power density, the vis upconversion luminescence intensities observed after 11000 and 9712 cm^{-1} excitation are unequal, see Figure 4. These two effects can quantitatively account for the different vis:NIR ratios observed after V^{3+} and Mo^{3+} excitation, and this shall be briefly illustrated for crystal (0.8/0.3): part d of Figure 4 shows that in this sample V^{3+} excitation at 11000 cm^{-1} leads to approximately a factor of 4 more vis Mo^{3+} $^2T_{2g} \rightarrow {}^4A_{2g}$ upconversion luminescence than Mo^{3+} excitation at 9712 cm^{-1}. On the other hand, there is also about a factor of 8 more near-infrared luminescence after 11000 cm^{-1} than after 9712 cm^{-1} excitation, see Figure 6. From this, 9712 cm^{-1} excitation is calculated to yield a vis:NIR luminescence ratio, which is a factor of 2 higher than for 11000 cm^{-1} excitation. This rough estimate is in good agreement with the factor of 1.6 in the bottom row of Table 5.

iii. Broadband near-Infrared (Lamp) Excitation. From the 15 K upconversion excitation spectra of crystals (0.1/0.3) and (0.2/4.3) in parts b and c Figure 4, we conclude that when exciting these samples with a laser source at one specific wavelength, this must occur into Mo^{3+} ^2E_g, $^2T_{1g}$ in order to obtain a maximum amount of visible upconversion luminescence. In other words, in these systems the V^{3+} codopants cannot improve the Mo^{3+} upconversion luminescence quantum yields under these experimental conditions. However, for broadband excitation between 9500 and 12500 cm^{-1} the situation is completely different. This becomes particularly obvious when comparing the 15 K upconversion excitation spectra of (0/0.3), part a of Figure 4, and the (0.8/0.3) crystal, part d of Figure 4. In these two crystals the Mo^{3+} dopant concentrations are identical, and thus the absolute intensities of their Mo^{3+} $^2T_{1g}$ excitation peaks in parts a and d of Figure 4 can in reasonable approximation be considered as equal. Thus, the integral of the excitation spectrum in part d of Figure 4 is roughly a factor of 60 higher than the integral of the spectrum in part a of Figure 4. Consequently, in crystal (0.8/0.3) broadband lamp excitation at 15 K is expected to yield about 60 times more visible upconversion luminescence than that released by crystal (0/0.3). This estimate is in good agreement with the experimental data in Figure 7. The output of a W-lamp below 12500 cm^{-1} is clearly capable to induce 15 K Mo^{3+} $^2T_{2g} \rightarrow {}^4A_{2g}$ upconversion luminescence in crystal (0.8/0.3), see part a of Figure 7, whereas for (0/0.3) it is below the detection limit, see part b of Figure 7. Thus, for broadband near-infrared excitation, the 15 K upconversion luminescence quantum yield of Mo^{3+} in Cs_2NaYCl_6 can be enhanced by at least an order of magnitude via V^{3+} codoping.

V. Conclusions

The upconversion data presented here demonstrate the feasibility of the principle, which includes the use of a broadband NIR absorber to sensitize sharp-line vis upconversion luminescence. Moreover it is shown that for broadband NIR excitation this approach may lead to order-of-magnitude enhancements of visible sharp-line upconversion luminescence quantum yields. Thus, the combination of transition metal broadband absorbers with either transition metal or rare earth upconversion ions may indeed yield new upconversion materials, which are potentially interesting candidates as luminescent materials for enhancing the efficiency of fluorescent lamps by converting their undesired (broadband) NIR output into vis radiation.

Our study of V^{3+} and Mo^{3+} codoped Cs_2NaYCl_6 represents only the starting point in the search for such materials. Several factors prevent V^{3+}:Mo^{3+}:Cs_2NaYCl_6 from having any application potential. The most severe deficiency of this system is the fact that Mo^{3+} upconversion luminescence is restricted to cryogenic temperatures. Obviously, for lamp phosphor applications materials with high luminescence quantum yields at room temperature and even above are required. Among transition metal ions only Re^{4+} is known to be an efficient room-temperature upconverter. Preliminary results on V^{3+}:Re^{4+}:Cs_2NaYCl_6 show that in this system V^{3+} broadband sensitization of visible Re^{4+} upconversion luminescence is possible even at room temperature.[61] Trivalent lanthanides such as Tm^{3+} or Er^{3+} are other, maybe more promising candidate ions for mixed broadband sensitizer/upconverter systems. First of all, these are very efficient room temperature upconverters. Second, their upconversion luminescence typically occurs in the blue or green spectral region, i.e., at substantially higher energies than in the case of Re^{4+}, which emits in the red.[34,62] However, VCl_6^{3-} is not a suitable sensitizer for Tm^{3+} or Er^{3+} upconversion, and therefore totally different sensitizer/host combinations will have to be explored in this context.

Another limitation of the V^{3+}:Mo^{3+}:Cs_2NaYCl_6 system is the fact that the V^{3+} near-infrared sensitization process is far from being optimal, mainly because $V^{3+} \rightarrow Mo^{3+}$ energy transfer is rather inefficient. As the present study shows, this is due to several factors. First of all the spectral overlap for this energy transfer process is small. Second, energy migration among the V^{3+} ions is inefficient. Consequently, excitation of V^{3+} ions which are spatially well separated from Mo^{3+} does not yield any ^2E_g-excited Mo^{3+} ions. Third, due to the elpasolite crystal structure with isolated MX_6^{3-} units, only multipole-multipole energy transfer processes are active in this system. Efficient (super-)exchange-mediated energy transfer processes such as for example in Mn^{2+} systems cannot take place.[63,64] This problem could potentially be overcome by choosing a host lattice in which neighboring metal ions share common bridging ligands. Interesting host systems in this context, in particular for trivalent metal ions, are found among the family of compounds $Cs_3M_2X_9$ with $X = Cl^-$ or Br^-.[65,68] A fully concentrated system such as for example $Cs_3V_2Cl_9$ would also display efficient energy migration along the sensitizer ions.[67] In addition, in strongly exchange-coupled sensitizer-upconverter systems the existence of a long-lived metastable excited state located on the sensitizer ion may not even be a necessity. At present this is only a hypothesis, but some support for this is given by recently explored upconversion phenomena in strongly exchange-coupled $Yb^{3+}-Mn^{2+}$ systems.[57,68,69]

The efficiency of the upconversion process itself is another crucial factor when aiming for materials applications. The inherent Mo^{3+} upconversion efficiency is very low even at 15 K, mainly due to the unfortunately low vis/NIR branching ratio from $^2T_{2g}$. Tm^{3+} and Er^{3+} do not suffer from this problem.

Regarding loss processes *after* the upconversion the V^{3+}:Mo^{3+}:Cs_2NaYCl_6 system exhibits very favorable properties. There is no quenching of Mo^{3+} upconversion luminescence by V^{3+}, because there is no spectral overlap of the Mo^{3+} $^2T_{2g}$ emissions with the V^{3+} ground state absorption. This is an extremely important point also to consider in the search for other

upconversion materials, in which a broadband absorber is combined with a rare earth ion. Many near-infrared broadband absorbers also absorb light in the visible spectral region, and they would thus immediately quench any visible upconversion luminescence. Additionally, inter-excited state luminescence transitions of the upconversion ion appearing at lower energies may spectrally overlap with ground-state absorptions of the sensitizer. This would lead to a reduction of the upconversion luminescence quantum yield. In V^{3+}:Mo^{3+}:Cs_2NaYCl_6 this is not the case because the only Mo^{3+} inter-excited-state transitions $^2T_{2g} \rightarrow {}^2T_{1g}/{}^2E_g$ occur below 5500 cm^{-1}, whereas all V^{3+} ground-state absorptions are above 9500 cm^{-1}. Most rare earth upconverters have many more energy levels in the visible and near-infrared spectral region than Mo^{3+} or Re^{4+}.[70] Consequently, there are usually multiple inter-excited-state luminescence transitions in spectral ranges spanning several thousands of wavenumbers. This increases the probability of (partial) cross-relaxation quenching.

In conclusion, there is both a practical and a fundamental interest in the study of the photophysical properties of systems, in which a broadband absorber is combined with an upconversion ion. We are currently exploring other combinations of transition metals and combinations of transition metal and rare earth ions.

Acknowledgment. We thank Patrick Reber for the crystal growth, Regina Schreier for the ICP measurements and G. Mackay Salley and Annina Aebischer for valuable discussions. This work was financially supported by the Swiss National Science Foundation.

References and Notes

(1) See for example: Dalton, L. R.; Harper, A. W.; Goshn, R.; Steier, W. H.; Ziari, M.; Fetterman, H.; Shi, Y.; Mustacich, R. V.; Jen, A. K.-Y.; Shea, K. J. *Chem. Mater.* **1995**, *7*, 1060.

(2) Bass, M., Ed. *Handbook of Optics*; McGraw-Hill: 1995; Vol. II, p 3.

(3) Ruillère, C. *Femtosecond Laser Pulses*, Springer-Verlag: Berlin, 1998.

(4) Macfarlane, R. M.; Tong, F.; Silversmith, A. J.; Lenth, W. *Appl. Phys. Lett.* **1988**, *52*, 1300.

(5) Joubert, M. F. *Opt. Mater.* **1999**, *11*, 181.

(6) Brede, R.; Heumann, E.; Koetke, J.; Danger, T.; Huber, G.; Chai, B. H. T. *Appl. Phys. Lett.* **1993**, *63*, 2030.

(7) Stephens, R. R.; Macfarlane, R. A. *Opt. Lett.* **1993**, *18*, 34.

(8) Chivian, J. S.; Chase, W. E.; Eden, D. D. *Appl. Phys. Lett.* **1979**, *35*, 124.

(9) Downing, E.; Hesselink, L.; Ralston, J.; Macfarlane, R. *Science* **1996**, *273*, 1185.

(10) Auzel, F. E. *Proc. IEEE* **1973**, *61*, 758.

(11) Wright, J. C.; *Topics in Applied Physics: Radiationless Processes in Molecules and Condensed Phases*; Fong, F. K., Eds.; Springer-Verlag: Berlin, 1976.

(12) Gamelin, D. R.; Güdel, H. U. In *Topics in Current Chemistry*, Yersin, H., Ed.; Springer-Verlag: Berlin, 2000; Vol. 214.

(13) Mita, Y. In *Phosphor Handbook*; Shionoya, S., Yen, W. M., Eds.; CRC Press: Boca Raton, 1999.

(14) Güdel, W. M.; Pollnau, M. *J. Alloys Compds.* **2000**, *303*−*304*, 307.

(15) Blasse, G.; Grabmaier, B. C. *Luminescent Materials*; Springer-Verlag: Berlin, 1994.

(16) Hüfner, S. *Optical Spectra of tRansparent Rare Earth Compounds*; Academic Press: New York, 1978.

(17) Kaplianskii, A. A., Macfarlane, R. M., Eds. *Spectroscopy of Solids Containing Rare Earth Ions*; North-Holland, Amsterdam, 1987; Vol. 21.

(18) Gamelin, D. R.; Güdel, H. U. *Acc. Chem. Res.* **2000**, *33*, 325.

(19) Flint, C. D.; Paulusz, A. G. *Mol. Phys.* **1981**, *44*, 925.

(20) Black, A. M.; Flint, C. D. *J. Chem. Soc., Faraday Trans. 2* **1975**, *71*, 1871.

(21) Flint, C. D.; Paulusz, A. G. *Chem. Phys. Lett.* **1979**, *62*, 259.

(22) Black, A. M.; Flint, C. D. *J. Mol. Spectrosc.* **1978**, *70*, 481.

(23) Flint, C. D.; Paulusz, A. G. *Mol. Phys.* **1980**, *41*, 907.

(24) Wermuth, M.; Güdel, H. U. *Chem. Phys. Lett.* **1997**, *281*, 81.

(25) Gamelin, D. R.; Güdel, H. U. *J. Am. Chem. Soc.* **2000**, *120*, 12143.

(26) Gamelin, D. R.; Güdel, H. U. *Inorg. Chem.* **1999**, *38*, 5154.

(27) Wermuth, M.; Güdel, H. U. *J. Chem. Phys.* **2001**, *114*, 1393.

(28) Wermuth, M.; Güdel, H. U. *J. Am. Chem. Soc.* **1999**, *121*, 10102.

(29) Möbert, P. E.-A.; Heumann, E.; Huber, G.; Chai, B. H. T. *Opt. Lett.* **1997**, *22*, 1412.

(30) Ostermayer, F. W.; van der Ziel, J. P.; Marcos, H. M.; van Uitert, L. G.; Geusic, J. E. *Phys. Rev. B* **1971**, *3*, 2698.

(31) Kück, S.; Diening, A.; Heumann, E.; Mix, E.; Sandrock, T.; Sebald, K.; Huber, G. *J. Alloys Compd.* **2000**, *300*−*301*, 65.

(32) Gamelin, D. R.; Salley, G. M.; Güdel, H. U. To be published.

(33) Kirk, A. D.; Furer, N.; Güdel, H. U. *J. Lumin.* **1996**, *68*, 77.

(34) Cresswell, P. J.; Robbins, D. J.; Thompson, A. J. *J. Lumin.* **1978**, *17*, 311.

(35) Wermuth, M.; Schmitz, A.; Güdel, H. U. *Phys. Rev. B* **2001**, *63*, 245118.

(36) Tanabe, Y.; Sugano, S. J. *J. Phys. Soc. Jpn.* **1954**, *9*, 753.

(37) Sugano, S.; Tanabe, Y.; Kamimura, H. *Multiplets of Transition Metal Ions in Crystals*; Academic Press: New York, 1970.

(38) Reber, C.; Güdel, H. U. *J. Lumin.* **1988**, *42*, 1.

(39) Gamelin, D. R.; Güdel, H. U. *J. Phys. Chem. B* **2000**, *104*, 10223.

(40) Knochenmuss, R.; Reber, C.; Rajasekharan, M. V.; Güdel, H. U. *J. Chem. Phys.* **1986**, *85*, 4280.

(41) Davis, C. C. *Laser and Electrooptics*; Cambridge University Press: New York, 1996; pp 357−370.

(42) Ejder, J. *J. Opt. Soc. Am.* **1969**, *59*, 223.

(43) Reber, C.; Güdel, H. U. *Photochemistry and Photophysics of Coordination Compounds*; Yersin, H., Vogler, A., Eds.; Springer-Verlag: Berlin, 1987.

(44) Wenger, O. S.; Güdel, H. U. *J. Phys. Chem. B* **2001**, *105*, 4181.

(45) Jacobsen, S. M.; Güdel, H. U. *J. Lumin.* **1989**, *43*, 125.

(46) Wenger, O. S.; Güdel, H. U. *Inorg. Chem.* **2001**, *40*, 157.

(47) Stranger, R.; Moran, G.; Krausz, E.; Güdel, H. U.; Furer, N. *Mol. Phys.* **1990**, *69*, 11.

(48) Yao, Q.; Maverick, A. W. *Inorg. Chem.* **1988**, *27*, 1670.

(49) Egorov, S. A.; Skinner, J. L. *J. Chem. Phys.* **1995**, *103*, 1533.

(50) Strek, W.; Ballhausen, C. J. *Mol. Phys.* **1978**, *36*, 1321.

(51) Brunold, T. C.; Güdel, H. U. *Inorganic Electronic Structure and Spectroscopy*; Solomon, E. I., Lever, A. B. P., Eds.; Wiley: New York, 1999; pp 259−306.

(52) Riedener, T.; Krämer, K.; Güdel, H. U. *Inorg. Chem.* **1995**, *34*, 2745.

(53) Vanoy, T. C.; McPherson, G. L. *Chem. Phys. Lett.* **1988**, *143*, 51.

(54) Vasquez, S. O.; Flint, C. D. *Chem. Phys. Lett.* **1995**, *238*, 378.

(55) Pollnau, M.; Gamelin, D. R.; Lüthi, S. R.; Hehlen, M. P.; Güdel, H. U. *Phys. Rev. B* **2000**, *61*, 3337.

(56) Valiente, R.; Wenger, O. S.; Güdel, H. U. *J. Chem. Phys.* **2002**, *116*, 5196.

(57) Reinhard, C.; Gerner, P.; Valiente, R.; Wenger, O. S.; Güdel, H. U. *J. Lumin.* **2001**, *94*−*95*, 331.

(58) Reinhard, C.; Valiente, R.; Güdel H. U. *J. Phys. Chem. B* In press.

(59) Heer, S.; Wermuth, M.; Krämer, K.; Güdel, H. U. *Chem. Phys. Lett.* **2001**, *334*, 293.

(60) Heer, S.; Wermuth, M.; Krämer, K.; Güdel, H. U. *Phys. Rev. B* **2002**, *65*, 125112.

(61) Wenger, O. S.; Güdel, H. U. Unpublished results.

(62) Cockroft, N. J.; Jones, G. D.; Nguyen, D. C. *Phys. Rev. B* **1992**, *45*, 5187.

(63) Yamamoto, H.; McClure, D. S.; Marzzacco, C.; Waldman, M. *Chem. Phys.* **1977**, *22*, 79.

(64) Auerbach, R. A.; McPherson, G. L. *Phys. Rev. B* **1986** *33*, 6815.

(65) Meyer, G. L. *Prog. Solid State Chem.* **1982**, *14*, 141.

(66) Dönni, A.; Furrer, A.; Güdel, H. U *J. Solid State Chem.* **1989**, *81*, 278.

(67) Leuenberger, B.; Briat, B.; Canit, J. C.; Furrer, A.; Fischer, P.; Güdel, H. U. *Inorg. Chem.* **1986**, *25*, 2930.

(68) Valiente, R.; Wenger, O. S.; Güdel, H. U. *Phys. Rev. B* **2001**, *63*, 165102.

(69) Gerner, P.; Wenger, O. S.; Valiente, R.; Güdel, H. U. *Inorg. Chem.* **2001**, *40*, 4534.

(70) Dieke, G. *Spectra and Energy Levels of Rare Earth Ions in Crystals*, Crosswhite, H. M., Crosswhite, H., Eds.; John Wiley: New York, 1968.